A direct comparison of CVD-grown and exfoliated MoS$_2$ using optical spectroscopy

A direct comparison of CVD-grown and exfoliated MoS$_2$ using optical spectroscopy

G Plechinger[1], J Mann[2], E Preciado[2], D Barroso[2], A Nguyen[2], J Eroms[1], C Schüller[1], L Bartels[2] and T Korn[1]

[1] Institut für Experimentelle und Angewandte Physik, Universität Regensburg, D-93040 Regensburg, Germany
[2] Chemistry, Physics, and Materials Science and Engineering, University of California, Riverside, CA 92521, USA

E-mail: tobias.korn@physik.uni-regensburg.de

Abstract

MoS$_2$ is a highly interesting material, which exhibits a crossover from an indirect band gap in the bulk crystal to a direct gap for single layers. Here, we perform a direct comparison between large-area MoS$_2$ films grown by chemical vapor deposition (CVD) and MoS$_2$ flakes prepared by mechanical exfoliation from mineral bulk crystal. Raman spectroscopy measurements show differences between the in-plane and out-of-plane phonon mode positions in CVD-grown and exfoliated MoS$_2$. Photoluminescence (PL) mapping reveals large regions in the CVD-grown films that emit strong PL at room-temperature, and low-temperature PL scans demonstrate a large spectral shift of the A exciton emission as a function of position. Polarization-resolved PL measurements under near-resonant excitation conditions show a strong circular polarization of the PL, corresponding to a valley polarization.

Keywords: MoS$_2$, Raman spectroscopy, photoluminescence, excitons

(Some figures may appear in colour only in the online journal)

1. Introduction

In recent years, two-dimensional crystal structures [1] have attracted a lot of attention. Many layered crystals can be mechanically exfoliated to yield flakes of single-layer thickness, just as graphene can be prepared from graphite. Transition metal dichalcogenides such as MoS$_2$ and WS$_2$ are currently studied by many groups, as they show drastic changes of the band structure with reduction of the number of layers. For MoS$_2$, a transition from indirect to direct band gap was theoretically predicted [2] and experimentally observed [3, 4], making the material interesting for possible opto-electronic applications. The band structure of monolayer MoS$_2$ allows for optical generation and detection of a valley polarization [5]. Large excitonic effects are predicted due to the two-dimensional crystal structure [6]. Additionally, a number of studies demonstrated transistor [7] and memory devices [8] with attractive properties. The majority of experimental studies have been performed on MoS$_2$ flakes exfoliated from mineral bulk crystal. While this material is readily available

for fundamental research and even allows for preparation of prototypical integrated circuits [9], scalable application of atomically thin MoS$_2$ will require wafer-scale deposition of films with well-controlled properties. A number of different methods for preparation of large-area MoS$_2$ films have been developed in recent years. It was demonstrated that chemical exfoliation of bulk MoS$_2$, in combination with mild annealing, can yield thin films which show pronounced photoluminescence (PL) [10]. Another approach is based on the sulfurization of thin metallic Mo films in nitrogen [11] or Argon [12] atmosphere. Chemical vapor deposition (CVD) and physical vapor deposition of MoS$_2$ was reported for different substrates, including graphene [13], copper [14] and sapphire [15].

Here, we report on optical spectroscopy of large-area MoS$_2$ films grown by CVD on SiO$_2$. We utilize Raman spectroscopy, as well as PL spectroscopy at room temperature and low temperatures to directly compare the properties of these films to MoS$_2$ flakes prepared by mechanical

exfoliation. PL mapping reveals large regions in the CVD-grown films that emit strong PL at room-temperature, and low-temperature PL scans demonstrate a large spectral shift of the A exciton emission peak as a function of position. A strong circular polarization of the PL is observed under near-resonant excitation conditions at low temperature, indicating an optically oriented valley polarization. We find pronounced differences between the in-plane and out-of-plane phonon mode positions and linewidths in CVD-grown and exfoliated MoS_2, and a clear correlation between the Raman and PL spectra in the CVD-grown films.

2. Methods

2.1. Sample preparation and optical characterization

The synthesis processes for the MoS_2 growth is as follows: we use two alumina crucibles (Aldrich Z561738, 70 mm × 14 mm × 10 mm), one containing 0.55 g of MoO_3 (Aldrich 99.5%) and one containing 0.70 g of sulfur powder (Alfa 99.5%) as our Mo and S sources, respectively. These crucibles are placed in a quartz process tube (2 inch diameter), which is inserted into a three zone tube furnace (Mellen TT12), in which only the center zone is heated. A flow of nitrogen gas (99.999%) is used to purge the tube (5.0 SCFH) for 15 min after which the flow is reduced (0.5 SCFH). The crucible containing MoO_3 is placed at the center of the heated zone with the substrate placed across the middle of the crucible. The crucible containing sulfur is placed 30 cm away from the crucible containing MoO_3 in the upstream direction. Our substrate is a square (2 cm width) piece of a boron-doped Si(100) wafer with a 300 nm oxide layer (SUMCO). The substrate is cleaned prior to use by an IPA rinse followed by a piranha etch (three parts sulfuric acid to one part hydrogen peroxide (30%)) for 1 h. The center zone of the furnace is heated to 700 °C in 43 min, as measured by a type-K thermocouple at the outer surface of the process tube, while the sulfur is simultaneously heated to ~200 °C (due to the temperature gradient from the central heated zone) and is held at this temperature for 10 min. Subsequently, the furnace is turned off and allowed to cool naturally to 500 °C. Compressed air is then used to rapidly cool the furnace to room temperature. This procedure yields samples as shown in figure 1(*a*), where a deposition of material is clearly visible on a 10 mm wide strip along the center of the substrate. Optical microscopy reveals regions of uniform apparent color, indicating a constant MoS_2 layer thickness, which are about 300 μm wide, at the edges of this strip, see figure 1(*b*). The long axis of these regions is aligned with the nitrogen flow direction during growth. We will show below that a pronounced PL emission corresponding to single-layer MoS_2 is observed in these regions. At the edge of these regions, the continuous MoS_2 layer transitions to a disordered array of individual islands, which are mostly triangular in shape and show the same apparent color (figure 1(*c*)).

The mineral MoS_2 flakes used for comparison are prepared using the mechanical exfoliation method well-established for graphene. A *p*-doped silicon wafer with 300 nm SiO_2 layer and lithographically defined metal markers is used
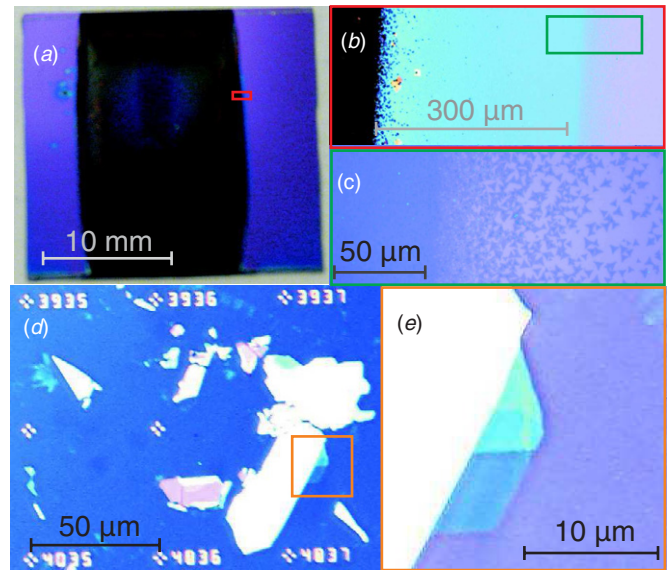

Figure 1. (*a*) Photograph of sample after CVD growth. (*b*) Optical micrograph of area indicated in (*a*) showing monolayer MoS_2 region. (*c*) High-magnification micrograph of area indicated in (*b*) showing the transition from individual islands to the monolayer. (*d*) Optical micrograph of MoS_2 flakes prepared by mechanical exfoliation on an SiO_2/Si wafer. (*e*) High-magnification micrograph of area indicated in (*d*). The bottom part of the flake (light blue color) is of monolayer thickness.

as a substrate. An optical microscope is used to identify flakes that contain single or few layer-regions based on the optical contrast [7, 16], the thickness of individual exfoliated flakes is determined by Raman spectroscopy based on the frequency difference of the characteristic Raman modes E_{2g}^1 and A_{1g} [17, 18]. Mechanical exfoliation yields a small number of single- and few-layer MoS_2 flakes with a size of several micrometers. Figure 1(*d*) shows a typical optical microscope image of flakes prepared by mechanical exfoliation, the larger-magnification image in figure 1(*e*) contains a flake with a single-layer region.

2.2. Optical spectroscopy

Raman spectroscopy measurements are performed at room temperature. For this, we utilize a microscope setup, in which a 532 nm cw laser is coupled either into a 100 × (1 μm laser spot size) or a 20 × (3 μm laser spot size) microscope objective, which also collects the scattered light in backscattering geometry. The scattered light is recorded using a grating spectrometer equipped with a cooled charge-coupled device sensor. A longpass filter is placed at the entrance of the spectrometer to suppress elastically scattered laser light. The sample is mounted on a motorized XY table and scanned under the microscope. Room-temperature PL measurements are performed using the same setup. For low-temperature PL measurements, the samples are mounted in vacuum on the cold finger of a small He-flow cryostat, which can also be scanned under the microscope. In PL and Raman scanning experiments, full spectra are collected for sample positions defined on a square lattice. For all the scans performed on the CVD-grown sample, the 20x microscope objective was
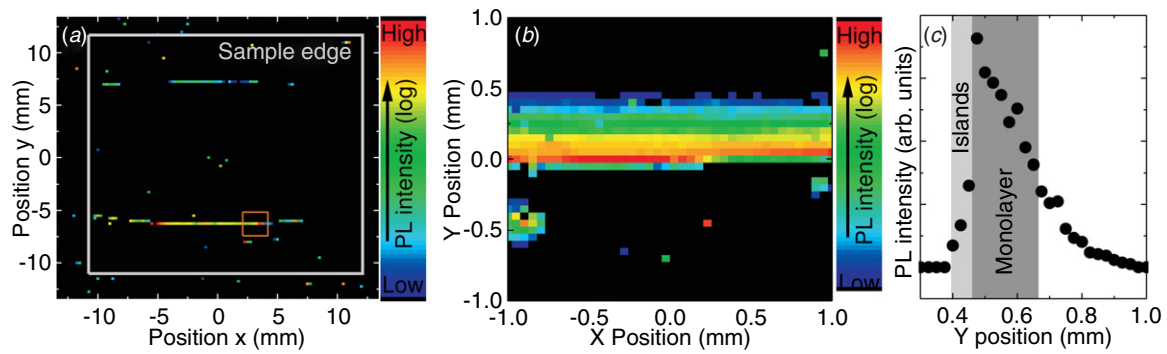
Figure 2. (*a*) False color plot of the A exciton PL intensity as a function of position on the CVD-grown sample measured at room temperature. The small orange square marks the region in which the higher-resolution scan shown in (*b*) was performed. (*b*) False-color plot of the A exciton PL intensity as a function of position. (*c*) High-resolution line scan of the A exciton PL intensity as a function of position along the vertical direction. PL data shown in (*b*) and (*c*) was collected at liquid-helium temperature.

utilized. An excitation density of about 170 kW cm^{-2} is used in the Raman and PL experiments, unless specified otherwise. In order to extract information from these spectra, an automated fitting routine is employed, which yields the integrated intensity, spectral position and full width at half maximum (FWHM) of the characteristic PL and Raman spectral features. To study valley polarization effects, near-resonant excitation is employed in the PL setup. For this, a tunable, frequency-doubled pulsed fiber laser system is utilized. Its center wavelength is tuned to 633 nm. This laser is circularly polarized by a quarter-wave plate and coupled into the microscope system. A longpass filter is utilized to suppress scattered laser light, and the circular polarization of the PL is analyzed using a second quarter-wave plate and a linear polarizer placed in front of the spectrometer.

3. Results and discussion

3.1. Photoluminescence

First, we discuss the PL spectra of the CVD-grown films and compare them to those of exfoliated MoS$_2$. Pronounced PL is observed only on single-layer MoS$_2$ flakes; PL yield for two and more layers of MoS$_2$ is significantly reduced and red-shifted with increasing number of layers [3, 4]. The characteristic PL emission observed in single-layer MoS$_2$ at room-temperature stems from the A exciton peak, which corresponds to a direct transition from the conduction band minimum to the uppermost valence band maximum at the K points in the Brillouin zone.

Figure 2(*a*) shows a false color plot of the A exciton PL intensity for the whole CVD-grown sample. The corresponding scanning PL measurement was performed using a step size of 250 μm. We note that strong PL, with an integrated intensity comparable to that of exfoliated flakes, is observed in two strip-like regions on the sample, each of which is about 8 mm long. The width of these strips cannot be discerned directly due to the low resolution of the large-area scan shown in figure 2(*a*). To study these regions in more detail, high-resolution scans were performed in the area denoted by the orange square in figure 2(*a*). False color plots created from such a scan, with a scan region of 2 mm and a step size of

50 μm, are shown in figure 2(*b*). This scan was performed at liquid-helium temperature. From this scan, we can determine the width of the region showing strong PL to be on the order of 200 μm, in agreement with the width of the regions showing homogeneous contrast observed in the optical microscopy. We also note that the increase of the PL intensity is gradual at the upper boundary of this region (corresponding to the transition from a monolayer covered with additional material to a bare monolayer of MoS$_2$), while it drops sharply at the bottom (corresponding to the transition from continuous monolayer to isolated islands and bare substrate). This behavior is also seen in the higher-resolution line scan of the PL intensity shown in figure 2(*c*). Thus, the areas of the CVD-grown samples which show PL comparable to single-layer MoS$_2$ flakes exceed the typical size of exfoliated flakes by several orders of magnitude, and allow for optical spectroscopy experiments without the use of high-resolution microscope objectives.

Now, we investigate the PL spectra in more detail. The PL data obtained in the scan shown in figure 2(*b*) allows us to extract the spectral position of the A exciton peak as a function of position on the sample. This is shown in figure 3(*a*) as a false color plot. We clearly see that the peak position shifts by more than 30 meV in the region which emits strong PL. This shift is pronounced in the direction perpendicular to the long axis of the region, while the peak position is nearly constant along the long axis. Individual spectra measured at different positions of the scan region are shown in figure 3(*b*), the positions P1–P3 are separated by 100 μm along the *y* direction. The vertical lines in figure 3(*b*) serve as a guide to the eye to mark maximum and minimum A exciton peak positions. The spectral shift indicates that the growth conditions, and the corresponding microscopic properties of the MoS$_2$ layer, change along the *y* direction. Three effects may contribute to this large spectral shift. It was shown theoretically by several groups that the band gap of MoS$_2$ can be strongly influenced by the application of strain, where biaxial compressive strain increases the band gap, while biaxial tensile strain decreases the band gap. The calculated values for band gap shift as a function of biaxial strain range from 105 to 190 meV/per cent [19–22]. A variation of the local biaxial strain can be generated during the growth process, which yields a temperature gradient across the substrate as the furnace is
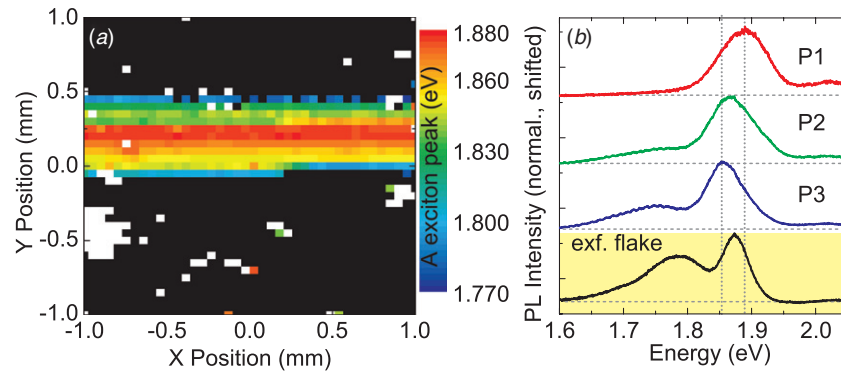
Figure 3. (*a*) False color plot of the spectral position of the A exciton PL peak. The scan area is identical to that shown in figure 2(*b*). (*b*) Normalized PL spectra measured on different positions of the scan region shown in (*a*) and on an exfoliated flake at liquid-helium temperature.

switched off. The observed shift of about 30 meV would correspond to a change of the local biaxial strain between 0.15% and 0.3%.

Additionally, it is very likely that there is a gradient of the Mo and S concentration across the substrate during growth, which may lead to local changes of the film composition. For example, a variation of the concentration of S vacancies would change the local carrier density. In *n*-doped MoS_2 layers, both, negatively charged excitons (trions) and neutral A excitons can be observed, with a binding energy of about 20 meV for the trions [23]. These two emission peaks typically merge due to their large linewidths, and the peak position of the resulting PL emission then depends on the relative contributions by excitons and trions. Transport measurements on our CVD-grown films indicate *n*-type conductivity [24], so that the observed PL emission may stem from a superposition of neutral and charged excitons, with a gradual change of the spectral weight due to changing carrier concentration. There may also be a locally varying deposition of amorphous S or Mo during growth, which would change the dielectric environment and modify the Coulomb screening. Recent calculations have yielded a very large binding energy of 0.85 eV for the A exciton in MoS_2 [6]. The exciton binding energy is proportional to ϵ^{-2}, therefore a change of the effective dielectric constant ϵ by 2% would account for a spectral shift of the A exciton emission of 30 meV.

In addition to the shift of the A exciton peak position, we also note that the FWHM of the peaks changes as a function of position, with values between 80 and 60 meV. Direct comparison of these PL spectra with a typical spectrum obtained from a single-layer MoS_2 flake at liquid-helium-temperatures demonstrates that the exfoliated MoS_2 has a significantly lower FWHM of about 37 meV. This indicates a larger inhomogeneous broadening of the A exciton transition in the CVD-grown sample due to local disorder, which cannot be resolved with the spatial resolution obtained in the PL experiment. In exfoliated MoS_2 flakes at low temperatures, we also observe a second, lower-energy PL peak (S exciton), which is associated with localized excitons bound to surface adsorbates [25, 26]. This peak is also observed in some areas of the CVD-grown sample, e.g., at position P3 and weakly at position P2, yet absent on the majority of the regions emitting
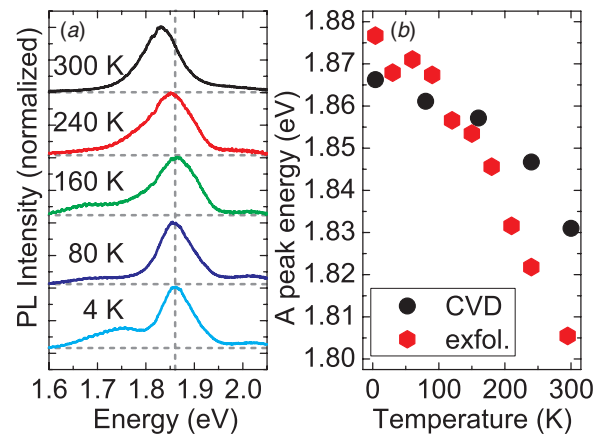

Figure 4. (*a*) Normalized PL spectra measured as a function of sample temperature. (*b*) A exciton peak position as a function of temperature for the CVD-grown sample (black dots) and an exfoliated MoS_2 flake (red hexagons).

strong PL. A complete suppression of this S exciton peak was previously observed in experiments on oxide-covered MoS_2 flakes [26], its absence on most of the CVD-grown sample may therefore indicate partial coverage of the CVD monolayer with additional material.

Next, we discuss the temperature dependence of the PL emission. Figure 4(*a*) shows a series of PL spectra measured on the CVD-grown sample for different sample temperatures. In order to avoid thermal drift of the sample position during changes of the temperature, a two-dimensional PL scan was performed at each temperature, and the spectra shown in figure 4(*a*) were created from these scans by averaging data in a 300 μm wide region. We note that the maximum of the A exciton emission redshifts by 35 meV in the temperature range from 4 K to 300 K, as shown in figure 4(*b*). Additionally, the spectral width of the A exciton emission increases with increasing temperature. By contrast, in exfoliated MoS_2 flakes, we observe a spectral redshift of the A exciton peak by 72 meV in the same temperature range. The redshift indicates a temperature-induced reduction of the band gap due to thermal expansion of the crystal lattice. The fact that the redshift is far less pronounced in the CVD-grown sample shows that the CVD-grown MoS_2 film strongly adheres to the SiO_2
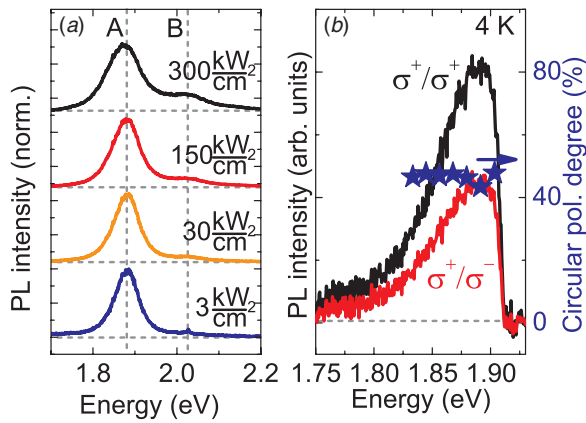
Figure 5. (*a*) Normalized PL spectra of the CVD-grown sample measured as a function of excitation density at room temperature. (*b*) Polarization-resolved PL spectra measured at liquid-helium temperature under near-resonant, circularly-polarized excitation, for co- and contra-circular excitation/detection helicities. The star symbols indicate the circular polarization degree of the PL as a function of energy.

substrate, which has a very small thermal expansion coefficient ($\alpha_{SiO_2} = 0.24 \times 10^{-6}$ K^{-1}) [27] compared to (bulk) MoS$_2$ ($\alpha_{MoS_2} = 1.9 \times 10^{-6}$ K^{-1}) [28]. A very similar reduction of the spectral shift with temperature was observed in oxide-covered MoS$_2$ flakes on SiO$_2$ substrates [26].

Excitation-density-dependent PL measurements of the CVD-grown sample performed at room temperature (see figure 5(*a*)) using the 532 nm laser show no significant changes of the spectral shape, A exciton peak position or linewidth from 2 kW cm^{-2} up to about 100 kW cm^{-2}. For further increases of the excitation density, we observe the emergence of a second, higher-energy PL peak, which becomes more pronounced as the excitation density is increased further. This peak corresponds to the B exciton (direct transition from the conduction band minimum to the lower valence band maximum at the K points in the Brillouin zone.) The emergence of the B exciton peak at high excitation densities is due to state-filling effects: the nonresonant excitation leads to the formation of both A and B excitons. For low excitation densities, however, most of the holes can relax to the upper valence band before photocarrier recombination, so that only A exciton PL emission is observed. At high excitation densities, the occupation of the upper valence band reduces the available states for this relaxation process, so that B exciton PL emission emerges. A similar behavior was recently observed also in exfoliated MoS$_2$ flakes [29].

Finally, we discuss the circular polarization of the PL of the CVD-grown sample at low temperatures. In monolayer MoS$_2$, the lack of an inversion center in the crystal structure leads to optical selection rules which allow for valley-selective excitation of electron–hole pairs either at the K$^+$ or the K$^-$ points in the Brillouin zone [5], depending on the photon helicity. If this optically generated valley polarization persists on the timescale of the photocarrier recombination time, it is directly observable in the circular polarization degree of the PL [30–33]. Figure 5(*b*) shows two PL spectra collected for co- and contra-circular excitation and detection under near-resonant excitation using the frequency-doubled pulsed fiber

laser system. In this experiment, the high-energy part of the A exciton emission is blocked by the longpass filter which is used to suppress the excitation laser. For co-circular excitation and detection, we note a significantly larger PL intensity than for contra-circular excitation and detection. From the two spectra, the circular polarization degree of the PL is calculated by dividing the difference of the PL intensities by their sum. For this, the PL intensities are spectrally averaged in 15 meV wide windows to reduce the noise. The circular polarization degree is plotted as a function of PL energy in figure 5(*b*). We find a near-constant value of more than 40% in the entire spectral range of the A exciton emission that is observable. This value is comparable to values we observe in exfoliated monolayer MoS$_2$ flakes under similar experimental conditions (not shown). Recently, it was demonstrated that the circular polarization degree strongly depends on the excess energy provided by the excitation laser [34]. The large circular polarization degree of the PL we observe is a clear indication that photocarrier excitation and recombination in the CVD-grown films follow the same selection rules as in mineral MoS$_2$. Therefore, these films will be highly useful for future studies of coupled spin and valley physics in monolayer MoS$_2$.

3.2. Raman spectroscopy

Now, we discuss the Raman spectra of the CVD-grown films and compare them to those of exfoliated MoS$_2$. For MoS$_2$ prepared by mechanical exfoliation, Raman spectroscopy is an excellent tool to map the number of layers in individual flakes. The most prominent Raman modes that can be observed in MoS$_2$ under nonresonant excitation are the E$^1_{2g}$ mode, which corresponds to an in-plane optical vibration of Mo and S atoms, and the A$_{1g}$, which is an out-of-plane optical vibration of the S atoms. The frequencies of both modes depend on the number of layers: while the A$_{1g}$ mode stiffens with additional layers, the E$^1_{2g}$ mode anomalously softens with additional layers [17]. This softening is attributed to enhanced dielectric screening [18]. Thus, the difference $\omega_{Diff} = \omega_{A_{1g}} - \omega_{E^1_{2g}}$ between the two modes can be used as a fingerprint for the number of layers. This technique is well-suited to differentiate between monolayers and flakes of up to four layers, while for thicker layers the mode positions approach the bulk limit. Thicker flakes can be differentiated by analyzing the frequency of the Raman shear mode, which also shows a strong dependency on the number of layers [35–37]. Recently, the effects of strain and carrier density on the Raman modes of MoS$_2$ were studied by several groups. Hui *et al* [38] observed a blueshift of E$^1_{2g}$ and A$_{1g}$ modes for biaxial compressive strain, while calculations show a redshift of both phonon modes with biaxial tensile strain [39]. In a top-gated MoS$_2$ transistor device, a clear dependency of the mode positions and amplitudes on the carrier density was observed [40]. With increasing carrier density, the A$_{1g}$ mode softens, while the E$^1_{2g}$ mode remains unaffected. Additionally, the relative intensity of the Raman modes changes. For low carrier density, the A$_{1g}$ mode is more intense than the E$^1_{2g}$ mode, for high carrier density, the intensity ratio reverses.

In order to determine the information that can be extracted from Raman spectra on the CVD-grown films, we performed
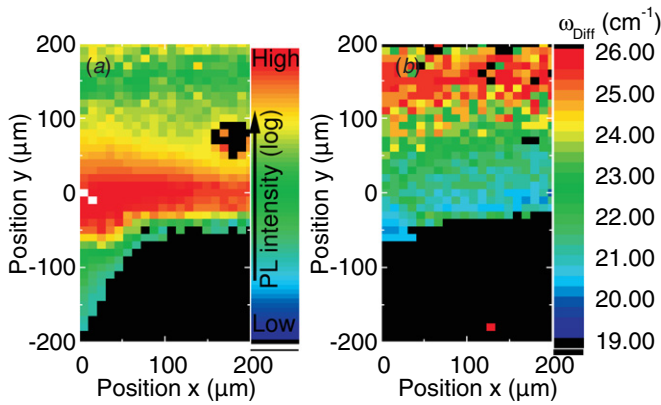
Figure 6. (*a*) False color plot of the A exciton PL intensity as a function of position on the CVD-grown sample measured at room temperature. (*b*) False color plot of the frequency difference of the A_{1g} and E^1_{2g} Raman modes as a function of position for the same scan area as shown in (*a*).
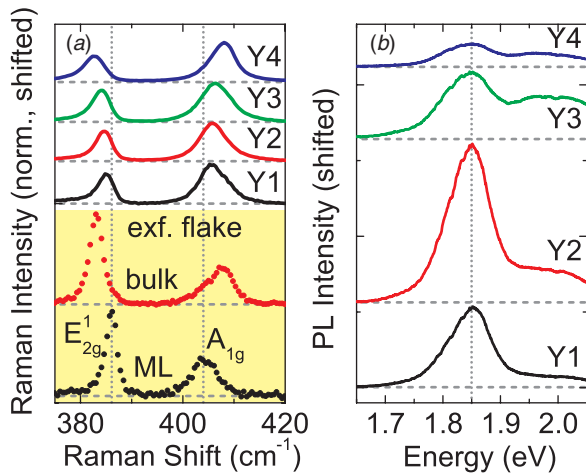

Figure 7. (*a*) Raman spectra measured on different positions of the CVD-grown film and on exfoliated monolayer (ML) and bulk-like flakes. All spectra are normalized to the amplitude of the A_{1g} mode. The vertical lines mark the positions of A_{1g} and E^1_{2g} in an exfoliated monolayer and serve as guide to the eye. (*b*) PL spectra measured on the same positions of the CVD-grown film as shown in (*a*).

combined Raman and PL scans at room temperature, so that for each spatial position, both, Raman and PL spectra were collected. False color plots created from these scans are depicted in figure 6. Here, the A exciton intensity is plotted in figure 6(*a*), this map is directly comparable to the frequency difference ω_{Diff} plotted in figure 6(*b*). Similar to the high-resolution PL scan shown in figure 2(*a*), we observe a rapid increase of the PL intensity along the vertical direction corresponding to the transition from bare substrate to islands and continuous film. In the corresponding frequency difference map, we see a gradual increase of ω_{Diff} along the vertical direction, with less well-defined contrast than in the PL intensity map.

We now discuss the Raman spectra in more detail. Figure 7(*a*) shows four Raman spectra collected at different positions on the CVD film, the corresponding PL spectra are depicted in figure 7(*b*). Here, the position Y1 corresponds to the film region where individual islands are observed in the

optical microscope, while Y2–Y4 are positions on different parts of the monolayer-like region. Let us first compare the Raman spectra to those collected from exfoliated flakes. All spectra shown in figure 7(*a*) are normalized to the A_{1g} mode amplitude. We clearly see that in the CVD-grown sample, the E^1_{2g} amplitude is smaller than the A_{1g}, while in the exfoliated flakes, the opposite is observed. From this observation, we can infer that the carrier density in the CVD-grown film may be significantly smaller than in the exfoliated flake [40]. Additionally, we note that the linewidths for both Raman modes in the CVD-grown film are larger than in the exfoliated flake, and the E^1_{2g} mode is asymmetric. The mode positions for the CVD-grown film are in between the values observed for monolayer and bulk-like exfoliated flakes. A small increase of the frequency difference ω_{Diff} (less than 0.5 cm^{-1}) is observed for the transition from isolated islands (Y1) to the film region showing the largest PL signal (Y2). The regions which emit less PL show further increase of the frequency differences, with position Y4 having a value of $\omega_{Diff} = 25$ cm^{-1}, comparable to bulk-like exfoliated MoS$_2$. For exfoliated MoS$_2$, however, a drastic reduction of the PL emission intensity, accompanied by a large redshift of the PL peak position, is observed for the change from monolayer to bilayer [3, 4] and thicker flakes. A variation of biaxial strain in the CVD-grown film from position Y1 to Y4 cannot explain the observed frequency difference change, as both E- and A-modes were shown to shift in the same direction as a function of strain [38, 39]. From the different evolution of ω_{Diff} and PL intensity we observe in the CVD-grown film, we infer that the Raman frequency shift is not caused by the formation of well-defined bilayer and multilayer regions, which would quench the PL due to a change of the band structure to an indirect band gap. By contrast, the monolayer may partially be covered by additional material which influences the dielectric screening and the vibronic properties, yet does not drastically change the band structure.

4. Conclusion

In conclusion, we have used Raman and PL spectroscopy to directly compare CVD-grown MoS$_2$ to exfoliated flakes. The CVD process used to prepare our films yields large areas which show PL comparable to monolayer MoS$_2$ flakes. In low-temperature PL measurements, we observe a spectral shift of the A exciton peak as a function of position. The linewidth of the A exciton is larger than that observed in exfoliated MoS$_2$. Some regions of the CVD-grown film also show PL emission associated with excitons bound to surface adsorbates. Temperature-dependent PL measurements reveal a small redshift of the A exciton peak, indicating that the CVD-grown MoS$_2$ adheres strongly to the SiO$_2$ substrate. In low-temperature PL experiments under near-resonant excitation, we observe a large circular polarization degree of the PL, commensurate with an optically induced valley polarization. In scanning Raman experiments, we observe a substantial shift of the characteristic Raman modes of MoS$_2$ in the region of the CVD-grown film which emits strong PL. This behavior differs from the Raman spectra observed in exfoliated MoS$_2$, where

similar shifts only occur for an increasing number of layers and a corresponding suppression of the PL due to changes in the band structure. Our observations indicate that the CVD-grown MoS_2 material is well-suited for future studies of exciton physics and valley effects. Further optimization of the growth process should yield even larger, homogeneous MoS_2 regions and may pave the way for device applications.

Acknowledgments

References

[1] Novoselov K S, Jiang D, Schedin F, Booth T J, Khotkevich V V, Morozov S V and Geim A K 2005 Two-dimensional atomic crystals *Proc. Natl Acad. Sci. USA* **102** 10451–3

[2] Lebègue S and Eriksson O 2009 Electronic structure of two-dimensional crystals from *ab initio* theory *Phys. Rev.* B **79** 115409

[3] Mak K F, Lee C, Hone J, Shan J and Heinz T F 2010 Atomically thin mos$_2$: a new direct-gap semiconductor *Phys. Rev. Lett.* **105** 136805

[4] Splendiani A, Sun L, Zhang Y, Li T, Kim J, Chim C-Y, Galli G and Wang F 2010 Emerging photoluminescence in monolayer mos$_2$ *Nano Lett.* **10** 1271–5

[5] Xiao D, Liu G-B, Feng W, Xu X and Yao W 2012 Coupled spin and valley physics in monolayers of mos$_2$ and other group-vi dichalcogenides *Phys. Rev. Lett.* **108** 196802

[6] Ramasubramaniam A 2012 Large excitonic effects in monolayers of molybdenum and tungsten dichalcogenides *Phys. Rev.* B **86** 115409

[7] Benameur M M, Radisavljevic B, Hron J S, Sahoo S, Berger H and Kis A 2011 Visibility of dichalcogenide nanolayers *Nanotechnology* **22** 125706

[8] Bertolazzi S, Krasnozhon D and Kis A 2013 Nonvolatile memory cells based on mos$_2$/graphene heterostructures *ACS Nano* **7** 3246–52

[9] Wang H, Yu L, Lee Y-H, Shi Y, Hsu A, Chin M L, Li L-J, Dubey M, Kong J and Palacios T 2012 Integrated circuits based on bilayer mos$_2$ transistors *Nano Lett.* **12** 4674–80

[10] Eda G, Yamaguchi H, Voiry D, Fujita T, Chen M and Chhowalla M 2011 Photoluminescence from chemically exfoliated mos$_2$ *Nano Lett.* **11** 5111–6

[11] Zhan Y, Liu Z, Najmaei S, Ajayan P M and Lou J 2012 Large-area vapor-phase growth and characterization of mos$_2$ atomic layers on a sio$_2$ substrate *Small* **8** 966–71

[12] Lee K, Gatensby R, McEvoy N, Hallam T and Duesberg G S 2013 High performance sensors based on molybdenum disulfide thin films *Adv. Mater.* **25** 6699–702

[13] Shi Y *et al* 2012 van der waals epitaxy of MoS_2 layers using graphene as growth templates *Nano Lett.* **12** 2784–91

[14] Kim D, Sun D, Lu W, Cheng Z, Zhu Y, Le D, Rahman T S and Bartels L 2011 Toward the growth of an aligned single-layer mos$_2$ film *Langmuir* **27** 11650–3

[15] Wu S, Huang C, Aivazian G, Ross J S, Cobden D H and Xu X 2013 Vaporsolid growth of high optical quality mos$_2$ monolayers with near-unity valley polarization *ACS Nano* **7** 2768–72

[16] Castellanos-Gomez A, Agraït N and Rubio-Bollinger G 2010 Optical identification of atomically thin dichalcogenide crystals *Appl. Phys. Lett.* **96** 213116

[17] Lee C, Yan H, Brus L E, Heinz T F, Hone J and Ryu S 2010 Anomalous lattice vibrations of single- and few-layer mos$_2$ *ACS Nano* **4** 2695–700

[18] Molina-Sánchez A and Wirtz L 2011 Phonons in single-layer and few-layer MoS_2 and WS_2 *Phys. Rev.* B **84** 155413

[19] Scalise E, Houssa M, Pourtois G, Afanasev V and Stesmans A 2012 Strain-induced semiconductor to metal transition in the two-dimensional honeycomb structure of MoS_2 *Nano Res.* **5** 43–48

[20] Huang C-W, Feng J, Qian X and Li J 2012 Strain-engineered artificial atom as a broad-spectrum solar energy funnel *Nature Photon.* **6** 866

[21] Peelaers H and Van de Walle C G 2012 Effects of strain on band structure and effective masses in MoS_2 *Phys. Rev.* B **86** 241401

[22] Li T 2012 Ideal strength and phonon instability in single-layer MoS_2 *Phys. Rev.* B **85** 235407

[23] Mak K F, He K, Lee C, Lee G H, Hone J, Heinz T F and Shan J 2013 Tightly bound trions in monolayer MoS_2 *Nature Mater.* **12** 207–11

[24] Mann J *et al* 2013 Facile growth of monolayer MoS_2 film areas on SiO_2 *Eur. Phys. J.* B **86** 1–4

[25] Korn T, Heydrich S, Hirmer M, Schmutzler J and Schüller C 2011 Low-temperature photocarrier dynamics in monolayer MoS_2 *Appl. Phys. Lett.* **99** 102109

[26] Plechinger G, Schrettenbrunner F-X, Eroms J, Weiss D, Schüller C and Korn T 2012 Low-temperature photoluminescence of oxide-covered single-layer MoS_2 *Phys. Status Solidi* **6** 126–8

[27] Tsou C, Huang Y-S, Li H-C and Lai T-H 2005 Determination of thermal expansion coefficient of thermal oxide *Sensors Mater.* **17** 441–51

[28] El-Mahalawy S H and Evans B L 1976 The thermal expansion of 2*H*-MoS_2, 2*H*-$MoSe_2$ and 2*H*-WSe_2 between 20 and 800 °C *J. Appl. Crystallogr.* **9** 403–6

[29] Korn T, Plechinger G, Heydrich S, Schrettenbrunner F-X, Eroms J, Weiss D and Schüller C 2014 Optical characterization, low-temperature photoluminescence, and photocarrier dynamics in MoS_2 *MoS$_2$ Lecture Notes in Nanoscale Science and Technology* vol 21 ed Z M Wang (Berlin: Springer) pp 217–36

[30] Cao T *et al* 2012 Valley-selective circular dichroism of monolayer molybdenum disulphide *Nature Commun.* **3** 887

[31] Zeng H, Dai J, Yao W, Xiao D and Cui X 2012 Valley polarization in MoS_2 monolayers by optical pumping *Nature Nanotechnol.* **7** 490

[32] Mak K F, He K, Shan J and Heinz T F 2012 Control of valley polarization in monolayer MoS_2 by optical helicity *Nature Nanotechnol.* **7** 494

[33] Sallen G *et al* 2012 Robust optical emission polarization in MoS_2 monolayers through selective valley excitation *Phys. Rev.* B **86** 081301

[34] Kioseoglou G, Hanbicki A T, Currie M, Friedman A L, Gunlycke D and Jonker B T 2012 Valley polarization and intervalley scattering in monolayer MoS_2 *Appl. Phys. Lett.* **101** 221907

[35] Plechinger G, Heydrich S, Eroms J, Weiss D, Schüller C and Korn T 2012 Raman spectroscopy of the interlayer shear mode in few-layer MoS_2 flakes *Appl. Phys. Lett.* **101** 101906

[36] Zeng H, Zhu B, Liu K, Fan J, Cui X and Zhang Q M 2012 Low-frequency raman modes and electronic excitations in atomically thin MoS$_2$ films *Phys. Rev.* B **86** 241301

[37] Zhang X, Han W P, Wu J B, Milana S, Lu Y, Li Q Q, Ferrari A C and Tan P H 2013 Raman spectroscopy of shear and layer breathing modes in multilayer MoS$_2$ *Phys. Rev.* B **87** 115413

[38] Hui Y, Liu X, Jie W, Chan N Y, Hao J, Hsu Y-T, Li L-J, Guo W and Lau S P 2013 Exceptional tunability of band energy in a compressively strained trilayer MoS$_2$ sheet *ACS Nano* **7** 7126–31

[39] Scalise E, Houssa M, Pourtois G, Afanas'ev V V and Stesmans A 2012 First-principles study of strained 2D MoS$_2$ *Physica* E **56** 416–21

[40] Chakraborty B, Bera A, Muthu D V S, Bhowmick S, Waghmare U V and Sood A K 2012 Symmetry-dependent phonon renormalization in monolayer MoS$_2$ transistor *Phys. Rev.* B **85** 161403